Article

Synthesis, Characterization, and Crystal Structure Determination of a New Lithium Zinc Iodate Polymorph $LiZn(IO_3)_3$

Zoulikha Hebboul[1], Christine Galez[2], Djamal Benbertal[1], Sandrine Beauquis[2], Yannick Mugnier[2], Abdelnour Benmakhlouf[3], Mohamed Bouchenafa[4], and Daniel Errandonea[5,*]

[1]Laboratoire Physico-Chimie des Matériaux (LPCM), University Amar Telidji of Laghouat, BP 37G, Ghardaïa Road, 03000 Laghouat, Algeria; z.hebboul@lagh-univ.dz (Z.H.); d.benbertal@lagh-univ.dz (D.B.)

[2]Univ. Savoie Mont Blanc, SYMME, F-74000 Annecy, France; Christine.Galez@univ-smb.fr (C.G); Yannick.Mugnier@univ-smb.fr (Y.M.); Sandrine.Beauquis@univ-smb.fr (S.B.)

[3]Laboratoire de caracterisation et Valorisation des Ressources Naturelles, Universite de Bordj Bou-Arreiridj, 34030 El-Anasser, Algeria; a.benmakhlouf@lagh-univ.dz (A.B.)

[4]Fundamental and Applied Physics Laboratory - Physics Departement, University of Blida 1, route de Soumaa BP 270, 09000 Blida, Algeria; mblasicom@yahoo.fr (M.B.)

[5]Departamento de Física Aplicada - ICMUV - MALTA Consolider Team, Universitat de València, c/Dr. Moliner 50, 46100 Burjassot (Valencia), Spain

* Correspondence: daniel.errandonea@uv.es

Abstract: Synthesis and characterization of anhydrous $LiZn(IO_3)_3$ powders prepared from an aqueous solution are reported. Morphological and compositional analyses were carried out by scanning electron microscopy and energy dispersive X-ray measurements. The synthesized powders exhibit a needle-like morphology after annealing at 400°C. A crystal structure for the synthesized compound has been proposed from powder X-ray diffraction and density-functional theory calculations. Rietveld refinements led to a monoclinic structure, which can be described with space group $P2_1$, number 4, and unit-cell parameters a = 21.874(9) Å, b = 5.171(2) Å, c = 5.433(2) Å, and β = 120.93(4)º. Density-functional theory calculations supported the same crystal structure. Infrared spectra were also collected and the vibrations associated to the different modes discussed. The non-centrosymmetric space group determined for this new polymorph of $LiZn(IO_3)_3$, the characteristics of its infrared absorption spectrum, and the observed second harmonic generation suggest a promising infrared non-linear optical material.

Keywords: iodate; crystal structure; x-ray diffraction; density functional theory; infrared absorption

1. Introduction

Metal iodates form a series of compounds potentially useful as dielectric materials and in non-linear optics [1-4]. They can also be employed for other applications like desalination and water treatment [5]. Among them, alkali-metal iodates [6], α-HIO_3 [7] and ammonium iodate [8] have attracted large attention not only because of their non-linear optical properties, but also due to their piezoelectric and pyroelectric response. For instance, lithium iodate ($LiIO_3$) has been widely used as a piezoelectric, acousto-optic, and second harmonic generation (SHG) material [9]. However, $LiIO_3$ crystals occasionally have OH inclusions, which reduce their transparency in the infrared (IR) region, affecting their performance [10] and their properties are known to strongly depend on the growth conditions [11]. Transition metal iodates, free of OH inclusions, e.g. $Zn(IO_3)_2$, have thus been developed as alternative materials with high SHG efficiency [12]. It is generally accepted that the important electro- and nonlinear optical properties of metal iodates originate from the lone electron pair of iodine in the IO_3^- iodate anion [13]. A lot of efforts have thus been dedicated to the synthesis of compounds containing this anion [14-19]. Iodates which combine two types of cations also

constitute a particular interesting group and for instance, attention has been devoted to the synthesis of double iodates like $LiFe_{1/3}(IO_3)_2$ [20], which exhibit higher nonlinear coefficients than $LiIO_3$ and transition metal iodates [21]. Among the double iodates, another material of special significance is $LiZn(IO_3)_3$, prepared in the past by solid-state sintering [22], and reported to be an excellent ionic conductor and to have a remarkable SHG. An orthorhombic structure was then proposed but the space group and atomic positions were not determined [22]. We report here a facile, cheap, and environmentally friendly synthesis route for anhydrous $LiZn(IO_3)_3$. A possible crystal structure is proposed based upon powder X-ray diffraction (XRD) experiments and Rietveld refinements. The structural determination is also supported by density-functional theory (DFT) calculations. Details of the morphology and IR spectral properties of the compound are also presented.

2. Materials and Methods

2.1 Sample preparation

The compound was synthesized from an aqueous solution of $LiIO_3$ (Sigma - Aldrich 99%) and $ZnCl_2$ (Riedel - de Haën 98%). Lithium iodate was first dissolved into 65% concentrated nitric acid obtained from Merck (4 mmol of $LiIO_3$ in 10 ml of 16N nitric acid) and then added to an anhydrous zinc chloride solution (1 mmol in 10 ml of 16N nitric acid). After being stirred thoroughly, the reaction mixture was slowly evaporated and maintained at 55 °C for four days leading to the formation of an amorphous white precipitate. After filtration and washing with de-ionized water the product was finally heat-treated at 400 °C for two hours in a tubular furnace.

2.2 Sample characterization

The synthesized samples were analyzed under scanning electron microscopy (SEM), powder X-ray diffraction (XRD), and Fourier transform infrared spectroscopy (FTIR). Phase purity and crystal structure of $LiZn(IO_3)_3$ crystals were evaluated by XRD from an Philips-Xpert pro diffractometer using Cu $K_{\alpha 1}$ (λ = 1.54056 Å) and $K_{\alpha 2}$ (λ = 1.54443 Å) radiation ($K_{\alpha 2}/K_{\alpha 2}$ ratio = 0.5), with a step size of $2\theta = 0.02°$ and sweeping with a 0.2º per minute velocity. The structural analysis was carried out using Powdercell [23]. For the structural refinement, the background was fitted with a six-order polynomial function and the peak profiles were modelled using a pseudo-Voigt function [24], using the Caglioti formula [25] for the angular dependence of the full-width at half-maximum of Bragg peaks. On the other hand, the refinement did not include the isotropic displacement factors which were assumed to be 1.0 $Å^2$, a typical value for lithium oxides and iodates [26-28], but adjusted an overall displacement factor [29]. Homogeneity and chemical composition of the samples were first assessed by SEM (VEGA\TESCAN) with a Peltier cooled XFlash™ silicon drift detector (model 410 M) for energy dispersive X-ray (EDX) analysis. Secondary electron images were recorded using 20 keV primary electrons. FTIR spectra (Jasco FT/IR-4200 instrument) were acquired after dispersing the $LiZn(IO_3)_3$ powder on a KBr carrier and a strong naked-eye SHG signal was observed from a collimated pulsed 1064 nm excitation laser (Wedge HB, Bright solutions, pulse width 1 ns, repetition rate 1 kHz) .

2.3 Density-functional theory calculations

Density-functional theory (DFT) is a quantum-mechanics calculation method that gives an accurate description of the structural and physical properties of oxides [30]. Accuracy of the results previously obtained by using DFT to different oxides [29, 31] supported its application in the case of $LiZn(IO_3)_3$. The DFT simulations here reported have been performed by using the *ab initio* plane-wave pseudopotential total-energy calculations as implemented in the CASTEP code [32]. This code has the advantage that partial atom occupancies (as in the compound here studied) can be easily implemented through the Project Explorer Tool. In the calculations, the exchange correlation energy was described in the general-gradient approximation (GGA) using the Perdew-Wang 1991(PW91) functional [33] with a kinetic cut-of energy of 500 eV for the plane-wave expansions. The reciprocal space integration was performed using 4 x 4 x 4 k-point grids in the Brillouin zone and the geometry optimization used the Broyden-Fletcher-Golfard-Shannon (BFGS) algorithm. Finally, the

Peer-reviewed version available at Crystals 2019, 9, 464; doi:10.3390/cryst9090464

total-energy is converged to less than 1 eV/atom and the Helmann-Fynmann forces on each atom are converged to less 0.01 eV/Å.

3. Results and discussion

3.1 Morphology and composition

Energy-dispersive X-ray spectroscopy (EDX) was used to confirm the composition and phase purity of the prepared $LiZn(IO_3)_3$ samples. Within the limits of experimental error, EDX analyses by both weight percent and atomic percent of Zn and I were found in agreement with their corresponding expected molar ratios (18.72(5)% and 31.60(5)%, respectively). The presence of impurities was not detectable within the resolution of the instrument. Fig. 1 shows the morphology and size of the synthesized material. As clearly evidenced from the scanning electron microscopy (SEM) micrograph, the raw powder is constituted of micron size needle-like particles. Their length varies between 10 and 100 μm and their diameter is smaller than 2 μm.

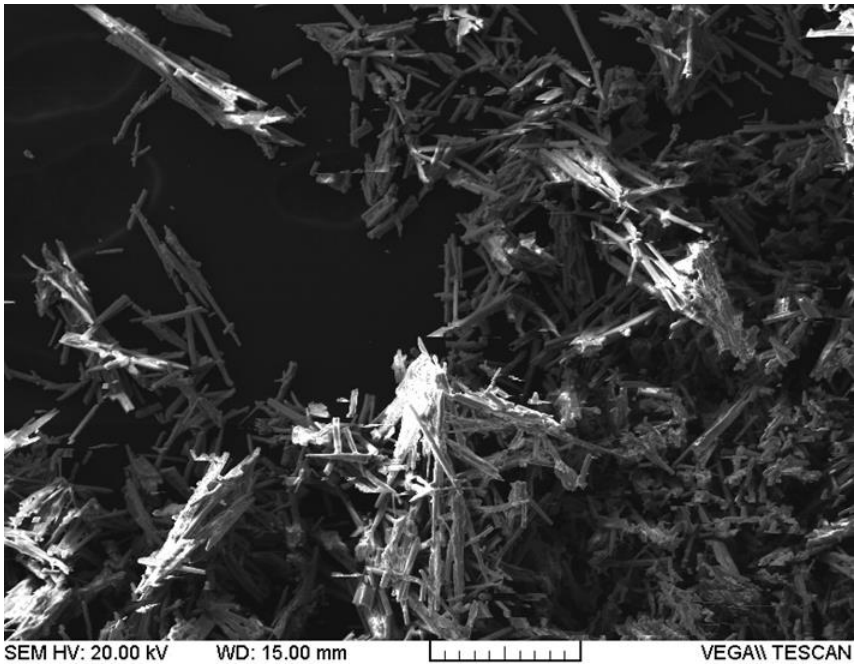

Figure 1. SEM morphology of the $LiZn(IO_3)_3$ powder. The ruler in the bottom part corresponds to 100 μm (10 μm/div).

3.2 Crystal structure

Fig. 2 shows a powder XRD pattern of $LiZn(IO_3)_3$, measured at room temperature. To obtain a phase-pure sample with the stoichiometric composition, we found that the initial Li:Zn molar ratio has to be increased above 4:1, as stated in the sample preparation section. An excess of Li is indeed necessary to prevent the formation of $Zn(IO_3)_2$ which is otherwise obtained when the Li:Zn ratio is typically below 2:1. It is also well noted that washing with water is required before annealing to remove any traces of the hygroscopic α-$LiIO_3$ that is also present after the evaporation step. A homogeneous and single phase material is then readily obtained and it differs from the well-known $Zn(IO_3)_2$, $ZnIO_3(OH)$ or α-$LiIO_3$ compounds [11, 26, 27, 34]. As in EDX measurements, phase impurities were not detected by XRD.

When analyzing the experimental XRD pattern, we found that it could not be indexed with the orthorhombic crystal structure previously reported by Sheng *et al.* [22]. By using the DICVOL routine, included in the FullProf Suite [35], we indexed the XRD pattern and found that the highest figure of merit corresponded to a monoclinic unit cell with parameters a = 21.747(9) Å, b = 5.201(2) Å, c = 5.435(2) Å, and β = 120.28(4)º. The analysis of the systematic extinctions ((0k0) reflections with k

Preprints (www.preprints.org) | NOT PEER-REVIEWED | Posted: 7 August 2019 doi:10.20944/preprints201908.0085.v1

Peer-reviewed version available at Crystals 2019, 9, 464; doi:10.3390/cryst9090464

odd are absent) indicated $P2_1$ as the possible space group. This space group is the same as that of the crystal structures of $Zn(IO_3)_2$ [26] and $Zn_2(IO_3)_4$ [27] (files number 54086 and number 415821 of the Inorganic Crystal Structure Database, ICSD) whereas $ZnIO_3(OH)$ belongs to the monoclinic space group *Cc* [34], number 9 (file number 185598 of ICSD). In addition, in the case of $Zn(IO_3)_2$, the unit-cell parameters b = 5.1158 Å, c = 5.469 Å, and β = 120º, are comparable with the lattice parameters b, c, and β we determined from our indexation of $LiZn(IO_3)_3$. The parameter a = 10.938 Å of $Zn(IO_3)_2$ is however approximately half the parameter a we obtained for $LiZn(IO_3)_3$.

Figure 2. XRD pattern of $LiZn(IO_3)_3$ measured using Cu $K_{\alpha 1}$ (λ = 1.54056 Å) and $K_{\alpha 2}$ (λ = 1.54443 Å) radiation. Dots correspond to the experiment. The Rietveld refinement carried out assuming

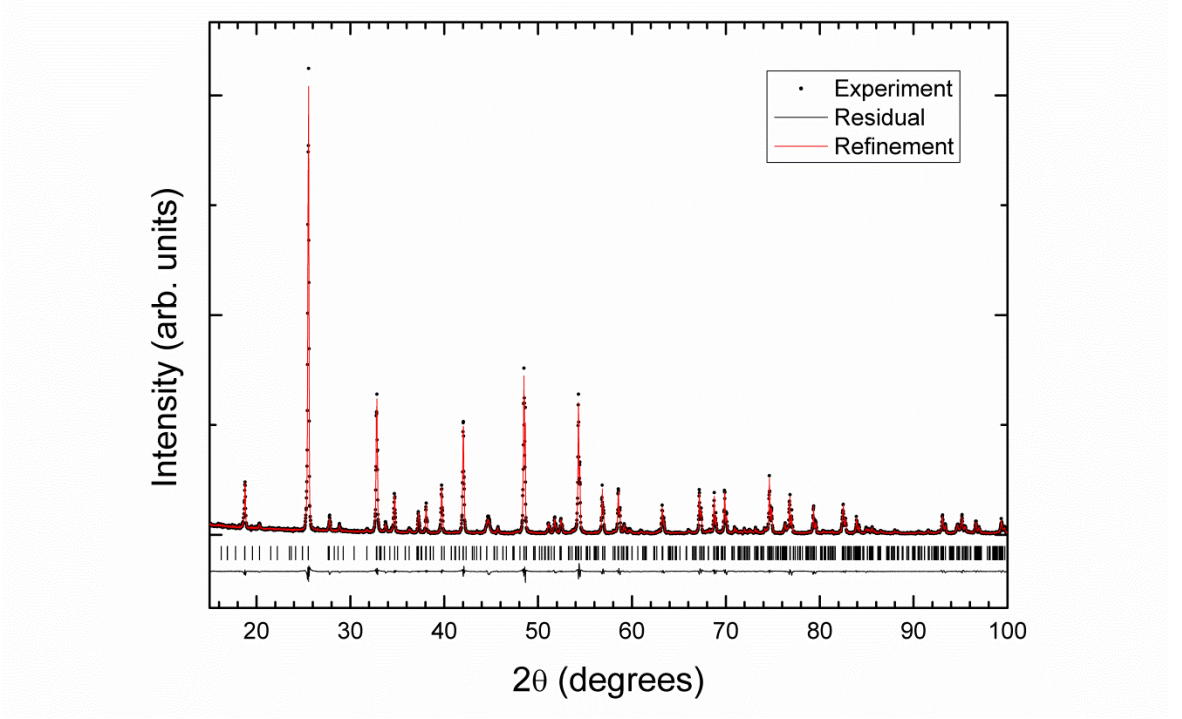

DFT-calculated atomic positions are shown with a red solid line. The residuals are plotted with a black solid line. Positions of the Bragg peaks are indicated by black ticks.

Based upon the similarities between the crystal structure of $LiZn(IO_3)_3$ and $Zn(IO_3)_2$, we have built a structural model for $LiZn(IO_3)_3$ by doubling the unit-cell of $Zn(IO_3)_2$ using the group-subgroup transformation tool available in PowderCell [23]. We then have assumed that Li and Zn ions alternatively occupy the positions generated from the original Zn positions and that I and O ions keep the same positions as in the original structure, but with an occupation factor of 0.75 (to be consistent with the compound stoichiometry). Starting from this model we have carried out a Rietveld refinement [35] and found that only the unit-cell parameters as well as the Li and Zn positions can be accurately determined in this way. In the refinement, positions of the I and O atoms have to be fixed though to the values obtained by doubling the unit-cell of $Zn(IO_3)_2$. This refinement procedure led otherwise to nonphysical results with some I-O bond distances too short and a reduced χ^2 smaller than 1. In order to optimize the above crystal structure determination we also have performed DFT calculations [36]. By considering our structural model (with space group $P2_1$) and the crystal structure of the other double iodates, we actually found that the above described structural model is the one leading to the lowest calculated enthalpy at ambient conditions. It is therefore the thermodynamically stable structure of $LiZn(IO_3)_3$ at ambient conditions. Additionally, the computer simulations not only provide information about the unit-cell parameters, but also on the atomic positions of all atoms which are summarized in Table 1. The DFT calculated unit-cell parameters are a = 21.945 Å, b = 5.048 Å, c = 5.487 Å, and β = 121.07º and agree within 1% with those previously obtained after the refinement of the XRD pattern. Consistency between the results

derived from XRD experiments and DFT calculations thus gives reliability to the proposed structural model of $LiZn(IO_3)_3$.

Table 1. Atomic positions calculated for the monoclinic $LiZn(IO_3)_3$ in the $P2_1$ space group.

Atom	Site	x	y	z	Occupation
Li	2a	0.13073	0.93865	0.02872	1
Zn	2a	0.62218	0.91685	0.00530	1
I_1	2a	0.03618	0.97718	0.33248	0.75
I_2	2a	0.53645	0.95209	0.33300	0.75
I_3	2a	0.30300	0.97387	0.33483	0.75
I_4	2a	0.79086	0.98644	0.32689	0.75
O_1	2a	0.45968	0.17690	0.33564	0.75
O_2	2a	0.95849	0.20846	0.28041	0.75
O_3	2a	0.10713	0.16625	0.67254	0.75
O_4	2a	0.60797	0.15273	0.65619	0.75
O_5	2a	0.05892	0.18401	0.08682	0.75
O_6	2a	0.54373	0.16225	0.03871	0.75
O_7	2a	0.38252	0.19763	0.66145	0.75
O_8	2a	0.86320	0.20816	0.63333	0.75
O_9	2a	0.22246	0.15968	0.31462	0.75
O_{10}	2a	0.70911	0.14574	0.29944	0.75
O_{11}	2a	0.30225	0.17019	0.03227	0.75
O_{12}	2a	0.78937	0.19692	0.01147	0.75

To go further, we then performed additional Rietveld refinements by using a different strategy, namely the atomic positions obtained from DFT calculations have been fixed in the structural model. The occupancies were also constrained to the values given in Table 1. The remaining parameters (for instance: unit-cell parameters, peak-shape parameters, overall displacement factor, scale factor) were then all refined, similarly to previous studies where the atomic positions of oxygen atoms were hardly determined without a similar approach [37, 38]. The structural model given in Table 1 finally leads to the smallest residuals (the R-factors are $R_P = 2.36\%$ and $R_{wp} = 3.18\%$ and a reduced χ^2 equal to 1.145) and a good-quality fit as illustrated in Fig. 2. The unit-cell parameters obtained after the new Rietveld refinement are $a = 21.874(9)$ Å, $b = 5.171(2)$ Å, $c = 5.433(2)$ Å, and $\beta = 120.93(4)^o$, with a fit accuracy that supports the assignment of the proposed monoclinic structure to the space group $P2_1$ [39 , 40]. It is also important to highlight here that the unit-cell volume (527.04 $Å^3$) of $LiZn(IO_3)_3$, which has a molar mass of 597.03 g/mol and 2 formula units per cell ($Z = 2$), is slightly smaller than twice the unit-cell volume of $Zn(IO_3)_2$ (265.02 $Å^3$). This could be a consequence of the partial occupation of the atomic sites of the iodine and oxygen atoms. Finally, as in other iodates, the determination of the exact position of the light Li atoms would deserve complementary neutron diffraction experiments [41].

Preprints (www.preprints.org) | NOT PEER-REVIEWED | Posted: 7 August 2019 doi:10.20944/preprints201908.0085.v1

Peer-reviewed version available at Crystals 2019, 9, 464; doi:10.3390/cryst9090464

The as-obtained crystal structure of $LiZn(IO_3)_3$ is shown in Fig. 3. In Table 2 we report the different interatomic bond distances. A structural comparison with the structures of $Zn(IO_3)_3$ and α-$LiIO_3$ [11, 26] shows that there are many similarities regarding polyhedral units and connectivity. In particular, the structure of the monoclinic polymorph of $LiZn(IO_3)_3$ can be described as a three-dimensional network of molecular ZnO_6 and LiO_6 octahedral units that are solely connected by monodentate iodate groups which have an asymmetric coordination. The IO_3 polyhedron exhibits the expected trigonal-pyramidal configuration with three different short I–O bond distances, which slightly change from one IO_3 polyhedron to another as can be seen in Table 2. These distances range from 1.9037(5) to 2.0833(5) Å. Each iodine atom has three additional oxygen neighbors, which are on the side of the lone-pair electrons of iodide. These weakly linked oxygen atoms are at longer distances with interatomic distances going from 2.1952 (5) to 2.7772(5) Å, thus forming a highly distorted IO_6 polyhedron. Regarding the ZnO_6 and LiO_6 octahedral units, they are slightly distorted with an average bond length of 2.168(3) and 2.155(3) Å, respectively. The quadratic elongation for the ZnO_6 (LiO_6) octahedron is 1.0064 (1.0052) and the distortion index is 0.01358 (0.01699). These two parameters, that are commonly used to describe distortions within a coordination octahedron, have been calculated using VESTA according to the definitions given by Robinson and Bauer [42].

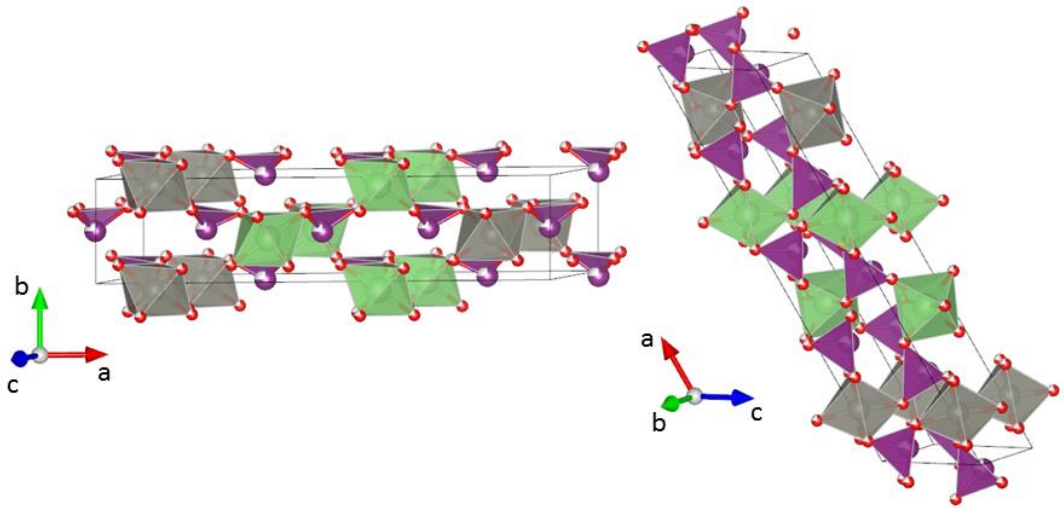

Figure 3. Schematic view of the crystal structure of $LiZn(IO_3)_3$. Zn (Li) atoms are shown in gray (green), I atoms in violet, and O atoms in red. The site occupation of the last two types of atoms is 0.75. The different coordination polyhedra are shown.

Table 2. Zn-O, Li-O, and I-O bond distances in the different coordination polyhedral of $LiZn(IO_3)_3$.

Zn-O	2.1087(5) Å	I_1-O	1.9571(5) Å	I_3-O	1.9249(5) Å
	2.2154(5) Å		1.9634(5) Å		1.9596(5) Å
	2.1391(5) Å		1.9758(5) Å		2.0833(5) Å
	2.1789(5) Å		2.4729(5) Å		2.4011(5) Å
	2.1828(5) Å		2.5285(5) Å		2.5406(5) Å
	2.1834(0) Å		2.6350(5) Å		2.7273(5) Å
Li-O	2.0903(5) Å	I_2-O	1.9450(5) Å	I_4-O	1.9037(5) Å
	2.1310(5) Å		2.0061(5) Å		1.9702(5) Å
	2.1351(5) Å		2.0484(5) Å		2.0161(5) Å
	2.1626(5) Å		2.1952(5) Å		2.5582(5) Å
	2.1648(5) Å		2.2619(5) Å		2.7049(5) Å
	2.2487(5) Å		2.3999(5) Å		2.7772(5) Å

We would like to comment here on the fact that the monoclinic structure here reported is different than the orthorhombic structure previously reported [22]. One possibility is that diverse polymorphs were obtained because of the different chemical routes used in the synthesis (starting reagents, solvent, temperature, crystallization pathways, etc.). For instance, in lithium iodate the processing parameters have a key influence on the three different crystalline structures that can be stabilized at room temperature [43]. A second option which should not be excluded is the incorrect assignment of the crystal structure in the previous study [22]. Indeed, previously only the unit-cell parameters were specified, but not the space group and atomic positions. The authors reported that the unit-cell corresponds to 4 formula units, which implies a volume per formula unit 25% smaller than in $Zn(IO_3)_3$ and $LiIO_3$, which is unexpected since $ZnLi(IO_3)_3$ is a binary solution of them. In contrast, as we described above, the monoclinic structure here proposed has many similarities with the ones of $Zn(IO_3)_2$ and α-$LiIO_3$. This and the consistency with DFT calculations further support the crystal structure here reported.

In terms of functional properties, it is worth to mention that the new polymorph of $LiZn(IO_3)_3$ crystallizes in a polar space group ($P2_1$) and is therefore a potential material for SHG with similar functionalities as $LiIO_3$ and $Zn(IO_3)_2$ [44]. The $P2_1$ space group belongs to class 2 for which 8 (resp. 4) nonzero SHG coefficients are to be considered without (resp. with) Kleinman's symmetry. So far, an accurate assessment of the independent SHG coefficients and overall conversion efficiency could not be obtained because of the needle-like morphology. However, a bright green spot has been observed under a 1064 nm laser excitation on powder agglomerates, suggesting that the produced SHG signal is very strong. Another interesting specificity of $LiZn(IO_3)_3$ arising from its crystal structure is the number of vacant sites and the zig-zag polyhedral chains running parallel to the *a*-axis (see Fig. 3). Ionic conductivity as well as highly anisotropic compression and thermal expansion are thus expected [45-47]. Other properties as the bulk modulus can be estimated from empirical relations, assuming that compression is dominated by the ZnO_6 and LiO_6 octahedra, from the Zn-O and Li-O bond distances and the formal charge of Zn and Li [48]. The obtained value is 55 GPa. It agrees with the measured bulk modulus of α-$LiIO_3$ [49], being therefore a plausible estimation of the bulk modulus of $LiZn(IO_3)_3$.

3.3 FTIR spectroscopy

Results of Fourier-transform infrared spectroscopy (FTIR) measurements are now discussed. Fig. 4 shows the transmission spectrum in the 4000 – 400 cm^{-1} region with a zoom in the 900 – 500 cm^{-1} range as depicted in inset to facilitate the mode identification associated to the iodate anion. In the FTIR spectra we have automatically subtracted the CO_2 bands from atmosphere absorption although weak artifacts around 2300 cm^{-1} are still present in the corrected data. According to group theory, $LiZn(IO_3)_3$ has eighty-one IR-active modes (Γ = 41A + 40B), which are considerable more numerous than the fifty-one IR-active modes (Γ = 26A + 25B) of $Zn(IO_3)_2$. This leads to a broadening of the IR bands of $LiZn(IO_3)_3$ due to partial phonon overlaps.

The better near-infrared transparency of $LiZn(IO_3)_3$ than that of α-$LiIO_3$ can however be noticed [50]. In addition, the spectral frequency range at 4000 - 3200 cm^{-1} is very useful to witness the presence of OH groups [51]. Here, a very low content of residual OH bonds is observed in agreement with the acidic synthesis conditions used for the preparation of $LiZn(IO_3)_3$. On the other hand, substitution of Li^+ by H^+ ions is very unlikely since the specific O-H…O vibrations of similar intensity observed at about 590 and 730 cm^{-1} in $Li_{1-x}H_x(IO_3)$ are not detected [52]. The band located from 1900 cm^{-1} to 1250 cm^{-1} could correspond to the second overtone of phonons from the 900 - 600 cm^{-1} band [53] or to the presence of H_2O molecules [54] which is less probable after the crystallization step at 400 °C. Between 900 and 600 cm^{-1}, several absorption features at 607, 673, 729, 764, 803, and 877 cm^{-1} are noticed and denoted by ticks in the inset of Fig. 4. Additional absorption peaks below 600 cm^{-1} can also be seen at 506, 521, 540, and 566 cm^{-1}.

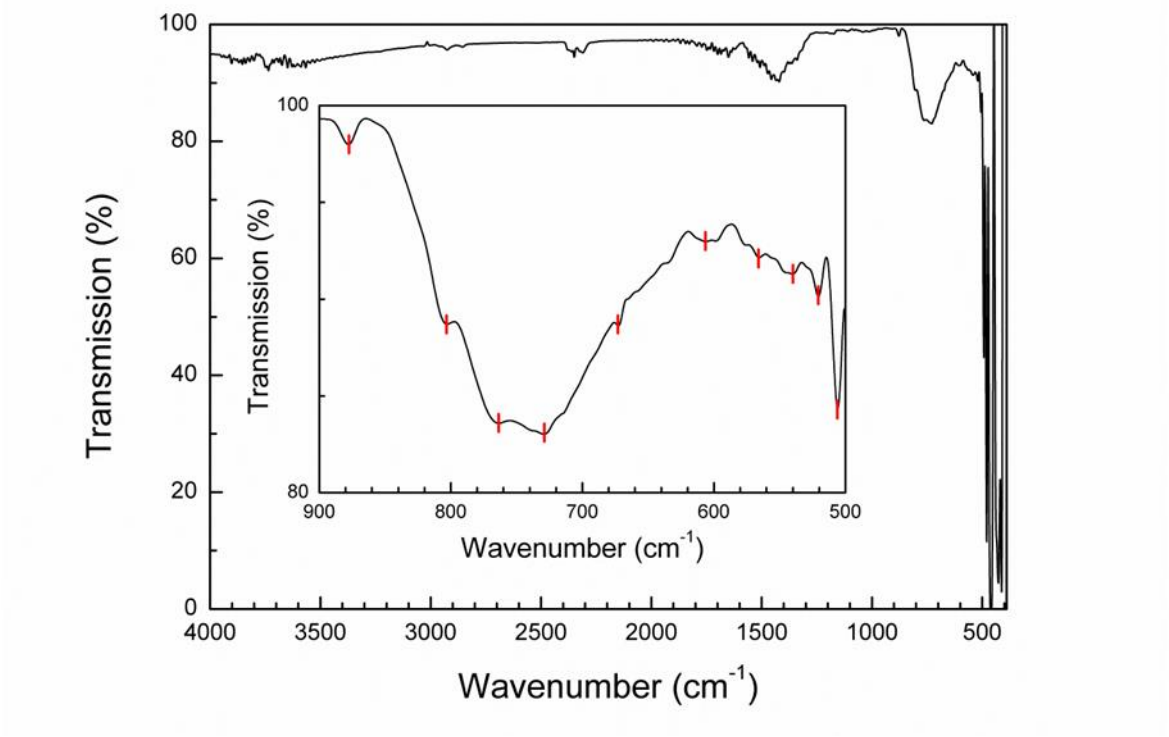

Figure 4. FTIR spectrum of $LiZn(IO_3)_3$ in the 4000 – 400 cm^{-1} region. The inset shows a zoom in the 900 – 500 cm^{-1} range. Ticks indicate position of the absorption peaks.

Regarding assignments of the iodate IR modes, we first remind that the vibrational frequencies of the symmetrical pyramidal IO_3^- ion in solutions and compounds are ν_1 (symmetric stretching) at 780 - 630 cm^{-1}, ν_2 (symmetric bending) at about 400 - 350 cm^{-1}, ν_3 (asymmetric stretching) at 820 - 730 cm^{-1}, and ν_4 (asymmetric bending) at about 330 cm^{-1} [51, 53, 54]. Here, presence of the distorted IO_6 polyhedral units as evidenced by XRD is expected to induce noticeable changes in the IR absorption spectrum of $LiZn(IO_3)_3$ comparatively to those of simple metal iodates. Two additional frequencies can be foreseen since degeneracy of the two asymmetric fundamental vibrations ν_3 and ν_4 is no longer present [51]. By analogy with other iodates, the five absorption peaks observed between 900 and 630 cm^{-1} can be assigned to the I–O stretching vibrations of the IO_3 polyhedron but occurrence in the $LiZn(IO_3)_3$ structure of pyramidal IO_3^- ions and of IO_6 octahedral units makes the IR spectra more complicate [12]. It is therefore difficult to assign the bands unambiguously, especially as the pyramidal and octahedral geometries are distorted. Finally, the absorption bands occurring between 673 and 500 cm^{-1} can be ascribed to the first overtones of the iodate ion bending modes with some lattice mode contributions involving vibrations between metal ions and IO_3 as a rigid unit.

4. Conclusions

A new polymorph of $LiZn(IO_3)_3$ was synthesized by a simple low-cost co-precipitation route and heat-treatment of the amorphous precipitate at 400°C. The combination of Rietveld refinements of the powder XRD pattern and DFT calculations results in a monoclinic crystalline lattice with the non-centrosymmetric space group $P2_1$. The unit-cell parameters and atomic positions were also determined. We also performed EDX and SEM measurements that confirm the phase purity and demonstrate that the synthesized $LiZn(IO_3)_3$ has a needle-like shape morphology. Finally, a FTIR analysis further supports the preparation of phase-pure $LiZn(IO_3)_3$ without occurrence of eventual H^+ ions. Because of the low symmetry of point group 2, a detailed assignment of each IR experimental frequency was not conducted but FTIR measurements were found consistent with other iodate compounds. More importantly, because of its non-centrosymmetric polar crystal

structure as well as its wide transparency and chemical stability compared to the very hygroscopic α-$LiIO_3$, $LiZn(IO_3)_3$ appears as a good candidate for non-linear optical applications. Besides, nanocrystal suspensions are under preparation so as to quantitatively assess, in the near future, the averaged SHG coefficients as already reported for other oxide nanomaterials [55].

Author Contributions: All authors contributed equally to this work; being all involved in experiments, analysis, interpretation of results, and writing of the manuscript.

Funding: This work was supported by the Spanish Ministry of Science, Innovation and Universities under grant MAT2016-75586-C4-1-P and by Generalitat Valenciana under grant Prometeo/2018/123 (EFIMAT). Y.M., S.B. and C.G. gratefully acknowledge support from the French-Swiss Interreg Program (NANOFIMT project).

Conflicts of Interest: The authors declare no conflict of interest.

References

1. S. P. Guo, Y. Chi, and G. C. Guo, Recent achievements on middle and far-infrared second-order nonlinear optical materials, *Coord. Chem. Rev.* **335** (2017) 44 - 57.
2. L. Xiao, Y. Zhenbo, J. Y. Yao, Z. S. Lin, and Z. G. Hu, A new cerium iodate infrared nonlinear optical material with a large second-harmonic generation response, *J. Mater. Chem. C* **5** (2017) 2130 - 2134.
3. A. H. Reshak and S. Auluck, $LiMoO_3(IO_3)$, a novel molybdenyl iodate with strong second-order optical nonlinearity, *J. Alloys Compd.* **660** (2016) 32 -38.
4. N. Ngo, K. Kalachnikova, Z. Assefa, R. G. Haire, and R. E. Sykora, Synthesis and structure of $In(IO_3)_3$ and vibrational spectroscopy of $M(IO_3)_3$ (M = Al, Ga, In), *J. Solid State Chem.* **179** (2006) 3824 - 3830.
5. D. Pathania, G. Sharma, N. Mu, and P. Vishal, A biopolymer-based hybrid cation exchanger pectin cerium(IV) iodate: synthesis, characterization, and analytical applications, *Desalin. Water Treatm.* **57** (2016) 468 - 475.
6. K. R. Biggs, R. A. Gomme, J. T. Graham, and J. S. Ogden, Characterization of molecular alkali metal iodates by mass spectrometry and matrix isolation IR spectroscopy, *J. Phys. Chem.* **96** (1992) 9738 - 9741.
7. K. Stahl and M. Szafranski, A neutron powder diffraction study of HIO_3 and DIO_3, *Acta Cryst. C* **48** (1992) 1571 - 1574.
8. E. T. Keve, S. C. Abrahams, and J. L. Bernstein, Pyroelectric ammonium iodate, a potential ferroelastic: crystal structure, *J. Chem. Phys.* **54** (1971) 2556 – 2563.
9. R. A. Kumar, D. R. Babu, R. E. Vizhi, N. Vijayan, and G. Bhagavannarayana, Synthesis, growth and optical studies of Mn: α-$LiIO_3$ single crystal, *Advanced Materials Research* **584** (2012) 3 - 7.
10. M. J. Bushiri, T. C. Kochuthresia, V. K. Vaidyan, and I. Gautier-Luneau, Raman scattering structural studies of nonlinear optical $M(IO_3)_3$ (M = Fe, Ga, α-In) and linear optical β-$In(IO_3)_3$, *J. Nonlin. Opt. Phys. Mater.* **23** (2014) 1450039.
11. Y. Mugnier, C. Galez, J. M. Crettez, P. Bourson, C. Opagiste, and J. Bouillot, Low-frequency relaxation phenomena in α-$LiIO_3$: The nature and role of defects, *J. Solid State Chem.* **168** (2002) 76 - 84.
12. T. C. Kochuthresia, I. Gautier-Luneau, V. K. Vaidyan, and M. J. Bushiri, Raman and FTIR spectral investigations of twinned $M(IO_3)_2$ (M = Mn, Ni, Co, and Zn) crystals, *J Appl. Spectrosc.* **82** (2016) 941 - 946.
13. P. Hermet, First-principles based analysis of the piezoelectric response in α-$LiIO_3$, Comput. Mater. Science **138** (2017) 199 - 203.
14. S. Peter, G. Pracht, N. Lange, and H. D. Lutz, Zinkiodate–schwingungsspektren (IR, Raman) und kristallstruktur von $Zn(IO_3)_2 \cdot 2H_2O$, *Z. Anorg. Allg. Chem.* **626** (2000) 208 -215.
15. A. L. Hector, S. J. Henderson, W. Levason, and M. Webster, Hydrothermal synthesis of rare earth iodates from the corresponding periodates: structures of $Sc(IO_3)_3$, $Y(IO_3)_3 \cdot 2H_2O$, $La(IO_3)_3 \cdot 1/2H_2O$ and $Lu(IO_3)_3 \cdot 2H_2O$, *Z. Anorg. Allg. Chem.* **628** (2002) 198 - 202.
16. B. Bentria, D. Benbertal, M. Bagieu-Beucher, A. Mosset, and J. Zaccaro, Crystal engineering strategy for quadratic nonlinear optics. Part II: $Hg(IO_3)_2$, *Solid State Sciences* **5** (2003) 359 - 365.
17. C. Galez, Y. Mugnier, J. Bouillot, Y. Lambert, and R. Le Dantec, Synthesis and characterisation of $Fe(IO_3)_3$ nanosized powder, *J. Alloys Compd.* **416** (2006) 261 - 264.
18. B. Bentria, D. Benbertal, Z. Hebboul, M. Bagieu-Beucher, and A. Mosset, Polymorphism of anhydrous cadmium iodate structure of ε-$Cd(IO_3)_2$, *Z. Anorg. Allg. Chem.* **631** (2005) 894 - 901.

19. C. F. Sun, C. L. Hu, X. Xu, J. B. Ling, T. Hu, F. Kong, X. F. Long, and J. G. Mao, $BaNbO(IO_3)_5$: A new polar material with a very large SHG response, *J. Am. Chem. Soc.* **131** (2009) 9486 - 9487.
20. Y. C. Lan, X. L. Chen, A. Y. Xie, P. Z. Jiang, and C. L. Lin, Synthesis, thermal and magnetic properties of new metal iodate: $(LiFe_{1/3})(IO_3)_2$, *J. Cryst. Growth* **240** (2002) 526 - 530.
21. L. Bonacina, Y. Mugnier, F. Courvoisier, R. Le Dantec, J. Extermann, Y. Lambert, V. Boutou, C. Galez and J.-P. Wolf, Polar $Fe(IO_3)_3$ nanocrystals as local probes for nonlinear microscopy, *App Phys B* **87** (2007) 399 – 403.
22. T. D. Sheng, F. Z. Ming, and L. W. Xiu, Invesigation of the pseudo-binary system $LilO_3$-$Zn(IO_3)_2$, *Acta Phys. Sinica* **30** (1981) 234 - 241.
23. W. Kraus and G. Nolze, POWDER CELL: a program for the representation and manipulation of crystal structures and calculation of the resulting X-ray powder patterns, *J. Appl. Cryst.* **29** (1996) 301 - 303.
24. A. B. Garg and D. Errandonea, High-pressure powder x-ray diffraction study of $EuVO_4$, *J. Solid State Chem.* **226** (2015) 147 – 153.
25. G. Caglioti, A. Paoletti. And F. P. Ricci, Choice of collimators for a crystal spectrometer for neutron diffraction, *Nucl. Instrum.* **3** (1958) 223 – 228.
26. J. K. Liang, and C. G. Wang, Diffusion of lithium in intercalated compound Li_xTiO_2, *Acta Chim. Sinica* **40** (1982) 969 - 976.
27. D. Phanon, B. Bentria, E. Jeanneau, D. Benbertal, A. Mosset, and I. Gautier Luneau, Crystal structure of $M(IO_3)_2$ metal iodates, twinned bypseudo-merohedry, with MII: MgII, MnII, CoII, NiII and ZnII, *Z. Kristallogr.* **221** (2006) 635 - 642.
28. J. M. Crettez, E. Coquet, J. Pannetier, J. Bouillot, and M. Durand-Le Floch, Neutron structure refinement of gamma- and beta-lithium: Comparison between alpha, gamma, and beta phases, J. Solid State Chem. **56** (1985) 133 – 147.
29. D. Errandonea, D. Santamaria-Perez, D. Martinez-Garcia, O. Gomis, R. Shukla, S. N. Achary, A. K. Tyagi, and C. Popescu, Pressure impact on the stability and distortion of the crystal structure of $CeScO_3$, *Inorg. Chem.* **56** (2017) 8363 - 8371.
30. A. Benmakhlouf, D. Errandonea, M. Bouchenafa, S. Maabed, A. Bouhemadou, and A. Bentabet, New pressure-induced polymorphic transitions of anhydrous magnesium sulfate, *Dalton Trans.* **46** (2017) 5058 – 5068.
31. R. Freccero, P. Solokha, D. M. Proserpio, A. Saccone, and S. De Negri, $Lu_5Pd_4Ge_8$ and $Lu_3Pd_4Ge_4$: Two more germanides among polar intermetallics, *Crystals* **8** (2018) 205.
32. S. J. Clark, M. D. Segall, C. J. Pickard, P. J. Hasnip, M. J. Probert, K. Refson, and M. C. Payne, First principles methods using CASTEP, *Zeitschrift für Kristallographie* **220** (2005) 567 - 570.
33. J. P. Perdew and Y. Wang, Accurate and simple analytic representation of the electron-gas correlation energy, *Phys. Rev. B* **45** (1992) 13244 – 13249.
34. D. W. Lee, S. B. Kim, and K. M. Ok, $ZnIO_3(OH)$: a new layered non-centrosymmetric polar iodate–hydrothermal synthesis, crystal structure, and second-harmonic generating (SHG) properties, *Dalton Trans.* **41** (2012) 8348 - 8353.
35. J. Rodriguez-Carvajal, Recent advances in magnetic structure determination by neutron powder diffraction, *Physica B* **192** (1993) 55 - 69.
36. R. Černý, Crystal structures from powder diffraction: Principles, difficulties and progress, *Crystals* **7** (2017) 142.
37. O. Gomis, J. A. Sans, R. Lacomba-Perales, D. Errandonea, Y. Meng, J. C. Chervin, and A. Polian, Complex high-pressure polymorphism of barium tungstate, *Phys. Rev. B* **86** (2012) 054121.
38. O. Gomis, B. Lavina, P. Rodríguez-Hernández, A. Muñoz, R. Errandonea, D. Errandonea, and M. Bettinelli, High-pressure structural, elastic, and thermodynamic properties of zircon-type $HoPO_4$ and $TmPO_4$, *J. Phys. Condens. Matter* **29 (**2017) 095401.
39. B. H. Tobby, R factors in Rietveld analysis: How good is good enough?, *Powder Diffr.* **21** (2006) 67 - 70.
40. D. Errandonea, R. S. Kumar, O. Gomis, F. J. Manjon, V. V. Ursaki, and I. M. Tiginyanu, X-ray diffraction study on pressure-induced phase transformations and the equation of state of $ZnGa_2Te_4$, *J. Appl. Phys.* **114** (2013) 233507.
41. P. G. Byrom and B. W. Lucas, Structure (neutron) of high-temperature phase I potassium iodate at 523 K, *Acta Cryst.* **C43** (1987) 1649 – 1651.

42. K. Momma and F. J. Izumi, VESTA: a three-dimensional visualization system for electronic and structural analysis, *Appl. Cryst.* **44** (2011) 1272 - 1276.
43. J. K. Liang, G. H. Rao, and Y. M. Zhang, Polymorphism phase transition and the relative stability of various phases in the $LiIO_3$ crystal, *Phys. Rev. B* **39**, (1989) 459 – 456.
44. C. L. Hu and J. G. Mao, Recent advances on second-order NLO materials based on metal iodates, *Coord. Chem. Rev.* **288** (2015) 1 - 17.
45. Y. Mugnier, C. Galez, J. M. Crettez, P. Bourson and J. Bouillot, Dielectric characterization and ionic conductivity of α-$LiIO_3$ crystals related to the growth conditions, *Sol. State. Comm.* **115** (2000) 619 - 623
46. D. Errandonea, A. Muñoz, P. Rodríguez-Hernández, O. Gomis, S. N. Achary, C. Popescu, S. J. Patwe, and A. K. Tyagi, High-pressure crystal structure, lattice vibrations, and band structure of $BiSbO_4$, *Inorg. Chem.* **55** (2016) 4958 - 4969.
47. A. B. Garg, D. Errandonea, J. Pellicer-Porres, D. Martinez-Garcia, S. Kesari, R. Rao, C. Popescu, and M. Bettinelli, *Crystals* **9** (2019) 2.
48. D. Errandonea and J. Ruiz-Fuertes, A brief review of the effects of pressure on wolframite-type oxides, *Crystals* **8** (2018) 71.
49. W. W. Zhang, Q. L. Cui, Y. W. Pan, S. S. Dong, J. Liu, and G. T. Zou, High-pressure x-ray diffraction study of $LiIO_3$ to 75 GPa, *J. Phys.: Condens. Matter* **14** (2002) 10579 – 10582.
50. M. S. Cafferty, Absorption of $LiIO_3$ in the infrared for the ordinary direction of propagation, *Infr. Phys. Techn.* **35** (1994) 801 - 804.
51. J. M. Crettez, R. Gard, and M. Remoissenet, Near and far infrared investigations from α and β lithium iodate crystals, *Solid State Commun.* **11** (1972) 951 - 954.
52. M. A. Pimenta, M. A. S. Oliveira, P. Boursond, and J. M. Crettez, Raman study of crystals, *J. Phys.: Condens. Matter* **9** (1997) 7903 – 7912.
53. K. Nassau, J. W. Shiever, and B. E. Prescott, Transition metal iodates. I. Preparation and characterization of the 3d iodates, *J. Solid State Chem.* **7** (1973) 186 - 204.
54. J. M. Crettez, J. P. Misset, and E. Coquet, Vibrations and force constants of the hexagonal lithium iodate crystal, *J. Chem. Phys.* **70** (1979) 4194 - 4198.
55. C. Joulaud, Y. Mugnier, G. Djanta, M. Dubled, J. C. Marty, C. Galez, J. P. Wolf, L. Bonacina, and R. Le Dante, Characterization of the nonlinear optical properties of nanocrystals by Hyper Rayleigh scattering, *J. Nanobiotechnology* **11** (2013) S8.